Title

MRI in systems medicine

Journal

WIREs Mechanisms of Disease, 12(1)

ISSN

1759-7684

Author

Liu, Thomas T

Publication Date

2020

DOI

10.1002/wsbm.1463

Peer reviewed

MRI in Systems Medicine

Thomas T. Liu *

Article Type:

Focus Article published in WIRES Systems Biology and Medicine;
https://doi.org/10.1002/wsbm.1463s

Abstract

Magnetic resonance imaging (MRI) is one of the primary medical imaging modalities and a key component of the standard of care in modern healthcare systems. One of the factors that distinguishes MRI from other imaging methods is the ability to program the MRI system to reveal a wide range of imaging contrasts, where each type of contrast offers unique information about the biological sample of interest. This ability stems from the fact that both the amplitude and phase of the magnetization of the underlying tissue can be manipulated to highlight different biological phenomenon. The flexibility and capabilities offered by modern MRI systems have enabled the development of a myriad of techniques for characterizing anatomy, physiology, and function. These include methods to characterize gross anatomy, tissue microstructure, bulk blood flow, tissue perfusion, and functional changes in blood oxygenation.

*Center for Functional MRI and Departments of Radiology, Psychiatry, and Bioengineering, University of California San Diego, La Jolla, CA, 92093

INTRODUCTION

Magnetic resonance imaging (MRI) is a widely used non-invasive biomedical imaging method for both clinical and research applications. For the past several decades it has been one of the primary medical imaging modalities and served as an important component of the standard of care in modern healthcare systems. Because of its non-invasive nature, it has also revolutionized research studies of anatomy, physiology, and function in humans and other animals. For example, functional MRI (fMRI) has led to tremendous gains in our understanding of brain function since its first demonstration in humans in 1992.

The field of MRI research is vast with over 550,000 publications listed in PubMed. Thus, any article on MRI can only scratch the surface of this large and continually growing area. In this paper, the goals are to briefly review the basic concepts of MRI and to demonstrate the use of these concepts in example applications of MRI to the study of anatomy, physiology, and function. In particular, we will focus on the important concepts of relaxation and phase. This article is aimed at the reader who is not only interested in the potential application of MRI to their area of study but also motivated to understand the physical concepts underlying the method. For this brief overview, we will make use of mathematical symbols and notation that are commonly used in MRI so as to help prepare the reader for further study in this area. At the same time, we will focus on providing the reader with an intuitive understanding of the key concepts.

MRI Basics

In this section we provide a very basic overview of how MRI works. Our goal is to present some key concepts that can be used to better understand the various MRI methods and applications that are presented in later sections.

Brief History

Magnetic resonance imaging (MRI) is based on the phenomenon of nuclear magnetic resonance (NMR), first reported in 1946 by Felix Bloch at Stanford University and Edward

Purcell at Harvard University. In 1952, Bloch and Purcell were awarded the Nobel Prize in Physics for their discovery. It would take another 20 years before Paul Lauterbur used linear magnetic field gradients to create the first magnetic resonance image, which was published in Nature in 1973. For his discovery Lauterbur shared the 2003 Nobel Prize in Medicine and Physiology with Sir Peter Mansfield, who made key contributions to the early development of MRI. After Lauterbur's initial discovery, the method was further developed in academic research labs during the 1970s. In the 1980s, partnerships between industry and academia led to the development of MRI systems for routine clinical use. The introduction of clinical MRI systems revolutionized the practice of radiology and to this day MRI continues to serve as one of the primary methods for non-invasive imaging of the human body.

Spin

MRI depends on two key properties of atomic nuclei: charge and spin, where the latter property refers to the intrinsic angular momentum of the nucleus. Nuclei with even numbers of both protons and neutrons exhibit zero spin. Nuclei with an odd number of protons and/or odd number of neutrons exhibit non-zero spin and are said to be NMR active. For biological systems, the NMR-active nuclei that are of interest are ^{1}H, ^{13}C, ^{19}F, and ^{31}P. However, for most MRI experiments the focus is on ^{1}H due to its large natural abundance.

A nucleus with spin can be thought of as a positively charged sphere rotating around its own axis. This rotating charged sphere can in turn be viewed as the superposition of many loops of current that collectively give rise to a magnetic moment $\vec{\mu} = \gamma\vec{S}$ that is proportional to the nuclear spin $\vec{S}$ where γ is the gyromagnetic ratio, a parameter that depends on the type of nucleus. The net magnetization $\mathbf{M}$ of a volume of interest is defined as the sum of the magnetic moments $\mathbf{M} = \sum_i \vec{\mu}_i$ in that volume. (See Table 1 for a glossary of symbols and terms).

If we consider a population of spins in the absence of an external magnetic field, there is no preferred direction for the spins. As a result, the vector sum of the moments is zero and there is no net magnetization, i.e. $\mathbf{M} = \sum_i \vec{\mu}_i = 0$. However, in the presence of an externally applied magnetic field, those magnetic moments that have a component in the same direction as the external field $\mathbf{B}_0$ will have lower energies than those moments that

have a component in the opposite direction. As an analogy, one can consider that a magnetic compass needle is in its lowest energy state when it it aligned with the earth's magnetic field and in its highest energy state when it points in a direction opposite to the earth's field.

In the presence of the external field, there will be relatively more spins "aligned" in the lower energy state, such that the net magnetization $\mathbf{M}$ is non-zero and aligned with the external field $\mathbf{B}_0$. This process is termed polarization and is depicted in Figure 1(a). At equilibrium (i.e. prior to any further manipulation of the magnetization), the magnetization is aligned with the external field and its magnitude $|\mathbf{M}_0| \propto B_0 P_D$ is proportional to the magnitude B_0 of the main field and the density P_D of nuclei, which is equivalent to proton density for ^{1}H imaging. By convention the axis of the external magnetic field is denoted as the z-axis and referred to as the *longitudinal* axis.

Magnetic Field Strength

Because the magnitude of the signal detected in MRI is proportional to the equilibrium magnetization, the sensitivity of the system increases with magnetic field strength B_0. At present, current clinical systems for human imaging operate at field strengths ranging from 0.2 to 7 Tesla (T), while advanced research systems may operate as high as 11.7 T. Preclinical systems for animal imaging typically range in strength from 4.7 T to 15.2 T, with the strongest system for in-vivo imaging operating at a field of 21.1 T. As a point of reference, the strength of the earth's magnetic field is roughly 50 μT. Thus, a 3 T system is 60,000 times stronger than the earth's field. The high fields used in MRI can exert extremely strong forces on ferromagnetic objects. A key safety requirement is to prohibit the introduction of ferromagnetic objects into the MRI environment.

Precession

All MRI methods rely on the manipulation (in both space and time) of the magnetization vector $\mathbf{M}$. The fundamental phenomenon that enables this manipulation is the precession of the magnetization about the main external magnetic field. Most readers will be familiar with the precession of a gyroscope or a spinning top. A top spinning on a flat surface rotates

about its own axis and also experiences an external torque due to gravity and the reaction force of the surface. The interaction of the angular momentum and the torque gives rise to the precession of the top about a vertical axis aligned with the gravitational force.

In MRI a collection of spins within a specified volume exhibits a bulk angular momentum $\mathbf{J}$ that is proportional to the net magnetization. The interaction of the angular momentum with the torque applied to the magnetization by the external field gives rise to precession of the magnetization about the axis of the external field. The frequency of precession occurs at the Larmor frequency $f = \frac{\gamma}{2\pi} B_0$. As a point of reference, the Larmor frequency of a hydrogen proton in a 3 T field is 127.7 MHz. In the United States, this frequency lies within the radiofrequency band used for air traffic control.

Radio Frequency Excitation

As mentioned above, at equilibrium the net magnetization $\mathbf{M}$ is aligned with the main field $\mathbf{B}_0$. In MRI, we would like to move the net magnetization away from its equilibrium position so that when it precesses about the main field it creates a time-varying magnetic field. By Faraday's law of induction, this time-varying field will induce a voltage in a receiver coil, which can be as simple as a loop of wire hooked up to an oscilloscope. Measurements of the induced voltage fluctuations constitute the MRI signal that is further processed to form images.

The process of perturbing the magnetization is called radio frequency (RF) excitation and involves the application of a secondary field $\mathbf{B}_1$ that is perpendicular to the main field. The magnitude of this secondary field is much smaller than the main field, and typically on the order of the earth's magnetic field strength (e.g. 50 μT). Because of its small size, the secondary field can do very little to perturb the magnetization when it is applied in a static fashion. However, if the field is applied in a rotating fashion where the frequency of rotation is equal to the Larmor frequency, it can effectively perturb the magnetization away from its equilibrium value. As an analogy, one may consider what it would take to perturb a 1 ton pendulum using just one's pinky finger. If the perturbations occur in a random fashion, the pendulum will barely budge. However, if the perturbations are applied at the resonant frequency of the pendulum, even a small force can eventually get the pendulum swinging.

For most applications, the RF excitation is performed in a relatively short time period (on the order of milliseconds), and the waveform used to perform the excitation is called an RF pulse. The RF pulse is said to "flip" the magnetization away from its equilibrium state along the z-axis. The angle between the resulting magnetization and the z-axis is termed the *flip angle*. Figure 1(b) shows the magnetization after excitation with a 90 degree flip angle. The magnetization lies completely within the x-y plane (denoted as the *transverse* plane) such that the longitudinal component $M_z = 0$ and the transverse component $M_{xy} = M_0$ is equal to the equilibrium magnetization.

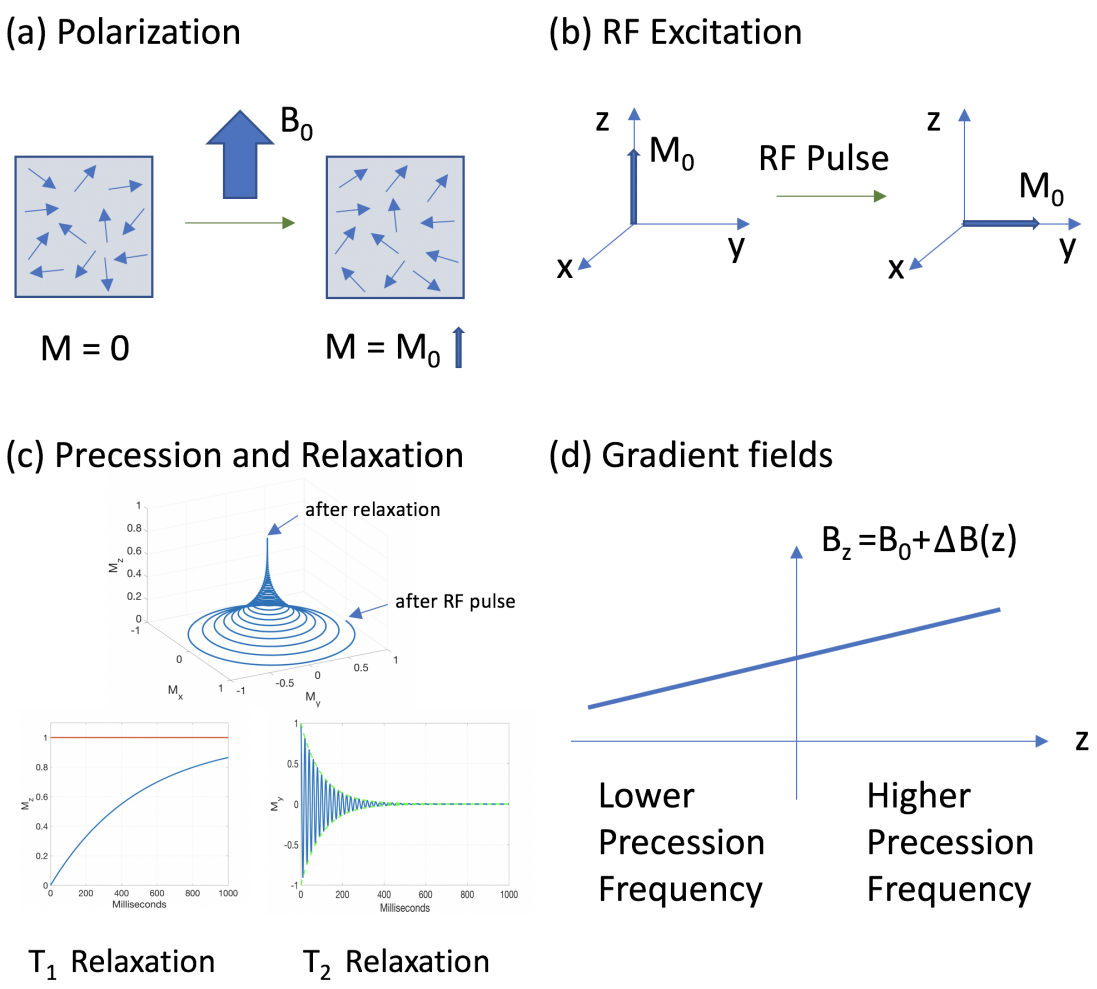

Figure 1: Key elements of an MRI experiment. (a) In the absence of an external magnetic field, there is no preferred direction for the spins and so the net magnetization is zero, as shown on the left. When the sample is placed in the presence of an external magnetic field $\mathbf{B}_0$ there is a tendency for the spins to align with the external field to create net magnetization that is aligned with the field, as shown on the right. (b) An RF pulse is used to tip the magnetization away from the external field. In this example, the magnetization is tipped into the transverse plane using an RF pulse with a 90 degree flip angle. (c) The tipped magnetization precesses around the main field and also exhibits both transverse and longitudinal relaxation. In the top plot, the magnetization starts off at $M_x = 0$, $M_y = 1$, $M_z = 0$ after the application of the RF pulse (where the magnetization values have been normalized by M_0 such that 1 denotes M_0). The magnetization precesses around the z-axis while at the same time exhibiting both T_1 and T_2 relaxation. The blue line in the lower lefthand plot depicts the return to equilibrium of the longitudinal component M_z of the magnetization with a time constant of T_1. The red line in the plot indicates the value of the equilibrium magnetization M_0. The upper envelope (dotted green line) in the lower righthand plot shows the magnitude $\sqrt{M_x^2 + M_y^2}$ of the transverse component decaying with a time constant of T_2. The lower envelope is provided to aid with the visualization of the overall envelope of the transverse component. The oscillating and decaying solid blue line in this plot depicts the M_y component. (d) Gradient fields are used to create spatial variations in magnetic field. Spins in regions with higher magnetic field will precess at a higher frequency as compared to spins in regions with a lower magnetic field.

Relaxation and Contrast

After the magnetization is perturbed from its equilibrium state, it will precess at the Larmor frequency about the main field while simultaneously returning back to its equilibrium state. This process is called relaxation and includes both an attenuation of the transverse component of the magnetization (i.e. the component perpendicular to the main field, denoted as M_{xy}) and a restoration of the longitudinal component (i.e. the component aligned with the main field, denoted as M_z). Longitudinal and transverse relaxation occur with time constants of T_1 and T_2, respectively. In general, $T_2 \ll T_1$, so that the decay of the transverse magnetization occurs more quickly than the recovery of the longitudinal magnetization. An example of this is depicted in Figure 1(c).

Differences between tissue types in the values of these time constants can be used to create contrast in MRI images. The image contrast is controlled through the specification of various timing and amplitude parameters, referred to as MRI pulse sequence parameters. Two of the most common types of image contrasts are T_1-weighted and T_2-weighted images, which emphasize differences in T_1 and T_2, respectively. Another common source of contrast is proton density. Tissues with a higher concentration of hydrogen protons will appear brighter than those with a lower concentration.

To demonstrate how a pulse sequence can be used to achieve contrast, we consider what is known as a spin-echo pulse sequence (Plewes, 1994). As shown in Figure 2(a), this pulse sequence is characterized by the use of a train of RF pulses with 90 degree flip angles, where the spacing between the pulses is termed the *repetition time* (TR). The longitudinal magnetization starts at zero immediately after each RF pulse and then recovers exponentially back towards equilibrium magnetization such that the longitudinal magnetization just prior to the next RF pulse is given by $M_z(0) = M_0\,(1 - \exp\,(-\mathrm{TR}/T_1))$. After each RF pulse, the transverse magnetization starts off with this value and then exponentially decays with a time constant of T_2, such that $M_{xy}(t) = M_z(0)\exp(-t/T_2)$. Because the longitudinal magnetization recovers from a saturated state (i.e. $M_z = 0$) immediately after each RF pulse, this type of pulse sequence is also referred to as a *saturation recovery* spin-echo pulse sequence.

By convention, the contrast is typically evaluated at a time $t = \text{TE}$, where TE denotes the echo time. In an MRI pulse sequence, the echo time refers to the time at which any imposed dephasing of the spins is "refocused" to obtain an "echo". In the depicted sequence, a refocusing RF pulse (denoted as 180 degree pulse) is used to address the effects of magnetic field inhomogeneities that can lead to dephasing of the magnetization. The resulting echo created by the refocusing pulse is called a *spin echo*. The process of refocusing is depicted in Figure 3. Putting together the various terms leads to the expression for the transverse magnetization $M_{xy}(\text{TE}) = M_0\left(1 - \exp\left(-\text{TR}/T_1\right)\right)\exp(-\text{TE}/T_2)$ obtained with the sequence parameters TE and TR.

There are three basic types of images that can be obtained with the spin-echo pulse sequence: (1) T_1-weighted, (2) T_2-weighted, and (3) proton density weighted images. For T_1-weighted images, the goal is to make the image sensitive to differences in T_1 and fairly insensitive to T_2. This can be achieved by using a short echo time (so that $\exp(-\text{TE}/T_2) \approx 1$) and choosing the TR to lie approximately halfway between the T_1 values of the tissues of interest. For T_2-weighted images, the goal is to make the image sensitive to differences in T_2 and fairly insensitive to T_1. This can be achieved by using a relatively long TR (so that $\left(1 - \exp\left(-\text{TR}/T_1\right)\right) \approx 1$) and choosing the TE to lie approximately halfway between the T_2 values of the tissues of interest. For proton density weighted images, the goal is to make the image insensitive to both T_1 and T_2 values. This can be achieved by using a relatively short TE and a relatively long TR, such that the resulting image is largely proportional to the equilibrium magnetization M_0 at each location. Examples of these different types of weighting are provided in Figure 2(b) and further discussed below in the section on anatomical imaging.

We should note that the spin-echo pulse sequence represents just one of many pulse sequence options that can be used to achieve contrast based on differences in relaxation rates. Other commonly used options include *inversion recovery* sequences and *rapid gradient-echo imaging* sequences. In an inversion recovery sequence a 180 degree RF pulse is used to invert the longitudinal magnetization M_z, such that M_z starts off at negative value (e.g. $-M_0$) before recovering to its equilibrium value. The imaging is then performed after some delay period, known as the inversion time (TI). With the proper choice of inversion time, the signal

from a specific tissue type can be nulled out (such that $M_Z(TI) = 0$) in order to better visualize pathology. For example, fluid attenuated inversion recovery (FLAIR) sequences are widely used clinically to better visualize lesions that might otherwise be obscured by the presence of signal from cerebrospinal fluid (Saranathan, Worters, Rettmann, Winegar, & Becker, 2017). Rapid gradient-echo imaging sequences are characterized by the use of a short TR and are widely used for applications, such as cardiac imaging, that benefit from the ability to rapidly acquire the needed data (Hargreaves, 2012).

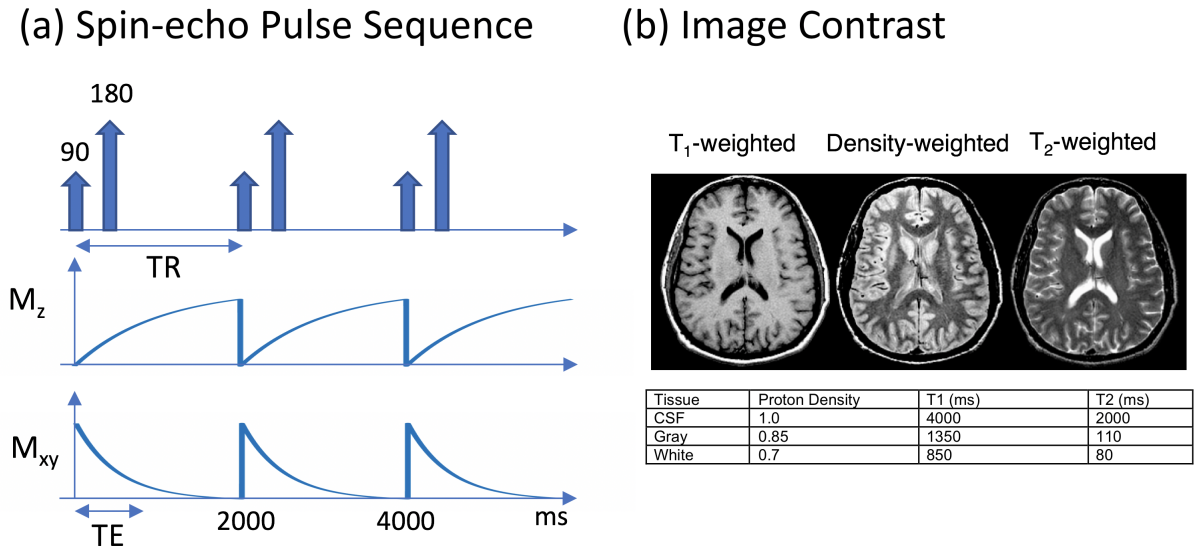

Tissue	Proton Density	T1 (ms)	T2 (ms)
CSF	1.0	4000	2000
Gray	0.85	1350	110
White	0.7	850	80

Figure 2: (a) Spin-echo pulse sequence. In the top row, the spacing between the 90 degree RF pulses is called the repetition time (TR). After the application of each 90 degree RF pulse, the magnetization is flipped from the longitudinal axis onto the transverse plane, such that $M_z = 0$. The longitudinal component then recovers exponentially and attains a value of $M_z(0) = M_0\,(1 - \exp(-\mathrm{TR}/T_1))$ just prior to the next 90 degree pulse. After each 90 degree pulse, the transverse magnetization starts out with this value and then exponentially decays with a time constant of T_2, such that $M_{xy}(t) = M_z(0)\exp(-t/T_2)$. The contrast of the sequence is evaluated at the echo time (TE). In this sequence a 180 degree refocusing pulse is used to create a spin echo. (b) Different types of image contrast can be achieved through the choice of values for TR and TE. The table lists typical proton density, T_1, and T_2 values for gray matter, white matter, and cerebrospinal fluid (CSF) at a field strength of 3 Tesla, where the proton density values are normalized by the CSF values. For the T_1-weighted image, the use of a short TE minimizes the sensitivity to T_2 and the choice of TR to lie halfway between the T_1 values of gray and white matter creates contrast between these two tissues types based on differences in T_1. For the density-weighted image, the use of a long TR and short TE makes the image relatively insensitive to T_1 and T_2, such that the resulting contrast largely reflects differences in proton density. For the T_2-weighted image, the use of a long TR and the choice of TE to lie halfway between the T_2 values of gray and white matter creates contrast between these two tissues types based on differences in T_2.

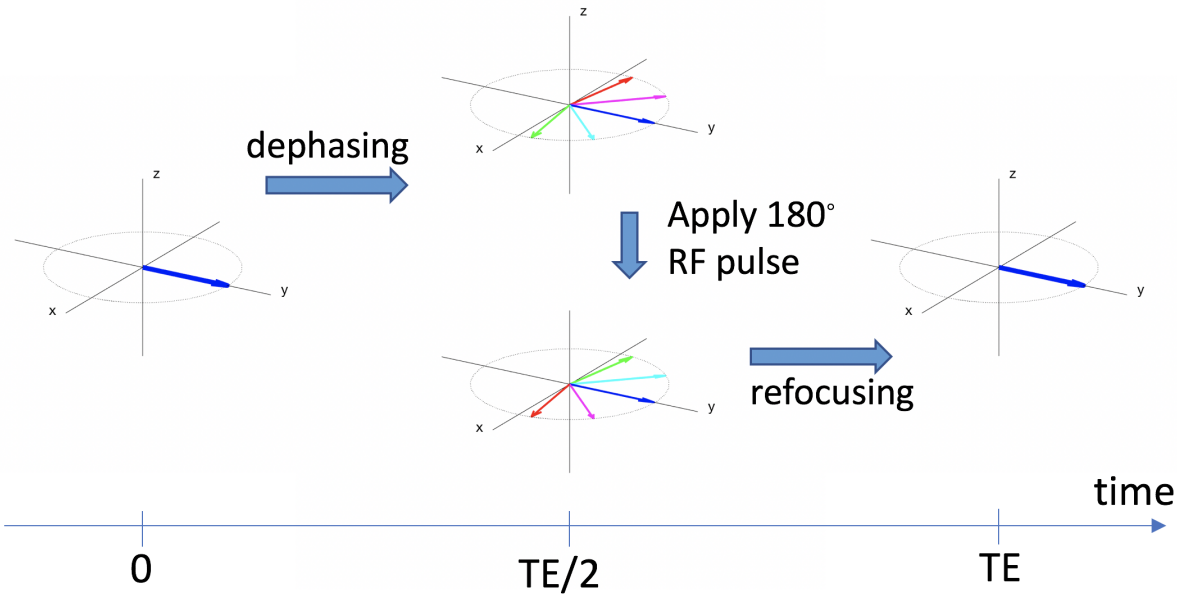

Figure 3: Formation of a spin echo. At the start of the experiment, the net magnetization (solid blue arrow) is fully aligned along the y-axis. Due to inhomogeneities in the magnetic field, spins will precess at different frequencies and acquire different phases. In this example, the green arrow in the upper middle plot depicts a spin that precesses at a higher frequency than the blue spin and has acquired a negative phase $\Delta\phi(\mathrm{TE}/2) = -\phi_0$ relative to the phase of the blue spin. The red arrow depicts a spin that precesses at a lower frequency and has acquired a positive relative phase $\Delta\phi(\mathrm{TE}/2) = +\phi_0$. The application of the 180 degree RF pulse inverts the signs of the relative phases of the spins such that in the lower middle plot the green spin now has a positive relative phase $\Delta\phi(\mathrm{TE}^{(+)}/2) = \phi_0$ and the red spin has a negative relative phase $\Delta\phi(\mathrm{TE}^{(+)}/2) = -\phi_0$. (Because it flips the relative phases of the spins, the action of the 180 degree RF pulse is sometimes referred to as a "pancake flip"). In the period after the application of the 180 degree RF pulse, the green spin will continue to precess at a higher frequency, and will thus resume accruing a negative relative phase, such that at time $t = \mathrm{TE}$ its relative phase will return to zero (i.e. $\Delta\phi(\mathrm{TE}) = \Delta\phi(\mathrm{TE}^{(+)}/2) - \phi_0 = 0$). In a similar fashion, the red spin will resume accruing a positive relative phase such that its phase $\Delta\phi(\mathrm{TE}) = \Delta\phi(\mathrm{TE}^{(+)}/2) + \phi_0 = 0$ also returns to zero at $t = \mathrm{TE}$. Thus, at time TE, the spins have been refocused and a spin echo has been formed.

Gradient Fields and Image Formation

As noted above, spins precess at the Larmor frequency, which depends on the local magnetic field. In general, it is desirable to make the main external magnetic field $\mathbf{B}_0$ as homogeneous as possible so that all spins of the same type precess at the same frequency. Lauterbur's key insight was to consider what happens when one adds a spatially-varying magnetic field such that spins at different spatial locations precess at different frequencies. For virtually

all MRI systems, the added field is a gradient field that varies linearly (with both negative and positive values) across space. The resulting frequency of precession is given by $f = \frac{\gamma}{2\pi}(B_0 + \Delta B(x, y, z))$ where $\Delta B(x, y, z)$ indicates the spatially varying incremental magnetic field imposed by the gradients. This approach is depicted in Figure 1(d).

By directly linking each spin's frequency to its spatial location, the use of linear gradient fields enables the formation of images. In the presence of a constant gradient field, the variation in frequencies causes the relative phases of the spins to exhibit spatial variations. This basic insight can be further developed to design the MRI acquisition such that acquired information is the spatial Fourier transform of the object. The image can then be formed simply by taking the inverse Fourier transform of the acquired data. In the context of MRI, the spatial Fourier domain is often referred to as *k-space*.

Figure 4 provides an overview of the basic ideas underlying the MRI acquisition and reconstruction process. The green dot in the upper righthand portion of Figure 4 indicates the point in k-space that is acquired when the spatial variation of phases shown in the lower right plot is imposed on the spins in the object. In practice time-varying gradient fields are used after each RF excitation to acquire information from multiple points in k-space. For rapid imaging applications, all the information needed to reconstruct an image can be acquired after a single RF excitation. However, the resulting images tend to have fairly low spatial resolution. To obtain images with higher spatial resolution, it is typically necessary to acquire the information in multiple passes, with each pass covering some portion of k-space. Figure 5 demonstrates the relationship between the extent of k-space information that is acquired and the spatial resolution of the reconstructed image. When the k-space coverage is limited to low spatial frequencies, as shown in the top row, the reconstructed image lacks fine spatial details and exhibits low spatial resolution. As the k-space coverage increases to include higher spatial frequencies (second and third rows), the fine spatial details are revealed and the resulting images exhibit increasingly higher spatial resolutions.

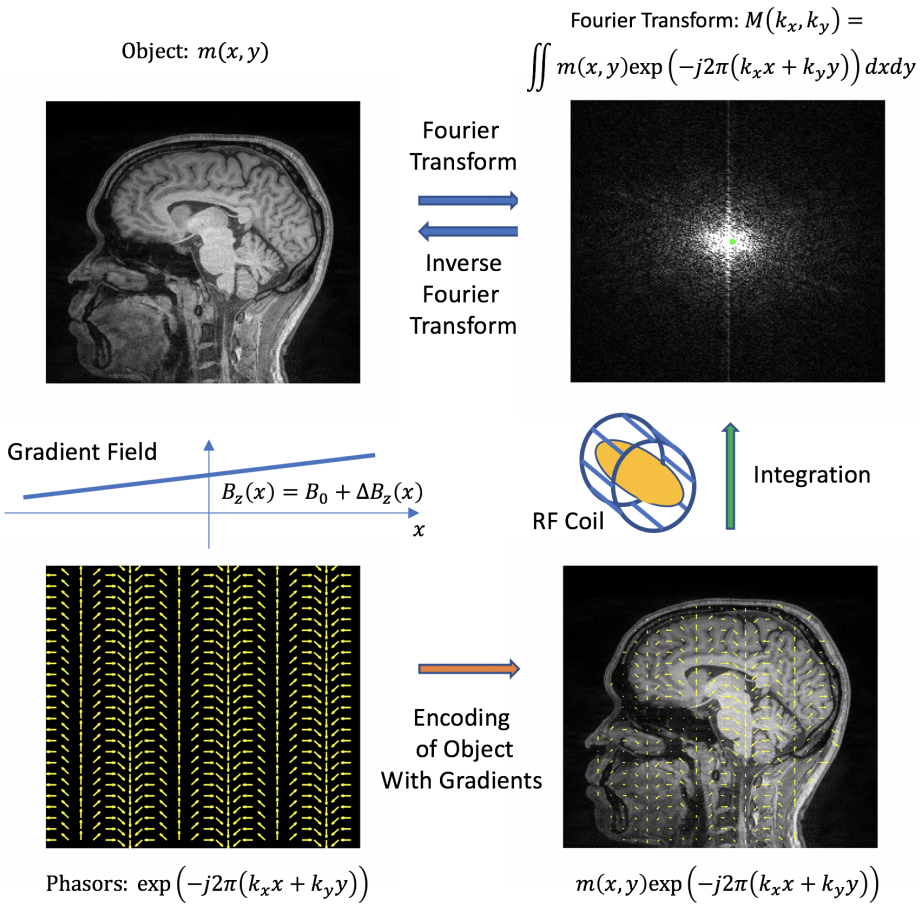

Figure 4: In a basic MRI study, the acquired information is the Fourier transform $M(k_x, k_y)$ of the object $m(x, y)$, where $m(x, y)$ denotes the transverse magnetization as a function of spatial location. To acquire this data, linear gradient fields are used to cause spins at different spatial locations to precess at different frequencies. The spatial variation in precession frequencies results in an associated spatial variation in the phases of the spins in the object. In the lower lefthand plot, a magnetic field gradient $\Delta B_z(x)$ along the x-axis produces a spatial variation in phase along the x-direction. This phase variation is represented mathematically using the phasor notation $\exp(-j2\pi(k_x x + k_y y))$, where k_x and k_y denote the spatial frequencies in the x and y directions, respectively. In this example $k_y = 0$ as there is no spatial variation of the phases in the y direction. Because the phase variation is imposed upon the transverse magnetization of the object, the encoding process can be represented as the product $m(x, y)\exp(-j2\pi(k_x x + k_y y))$ of the object and the phase variation. Integration of this product over space results in the Fourier transform $M(k_x, k_y)$ of the object at the spatial frequencies k_x and k_y. The integration is performed implicitly by the RF coil, which is sensitive to the magnetization from the entire volume (depicted as the yellow ellipsoid within the coil). The green dot in the upper righthand image indicates the point in k-space for which information is acquired using the phase variation shown in the lower lefthand plot. Over the course of an MRI scan, the information from many points in k-space is acquired. This is accomplished by manipulating the timing and amplitude of the gradients to impose different phase variations on the object (corresponding to different values of k_x and k_y) such that the acquisition process gradually fills in the values of the Fourier transform at different points in k-space. At the completion of the scan, an inverse Fourier transform is used to convert the Fourier transform samples into a representation of the object.

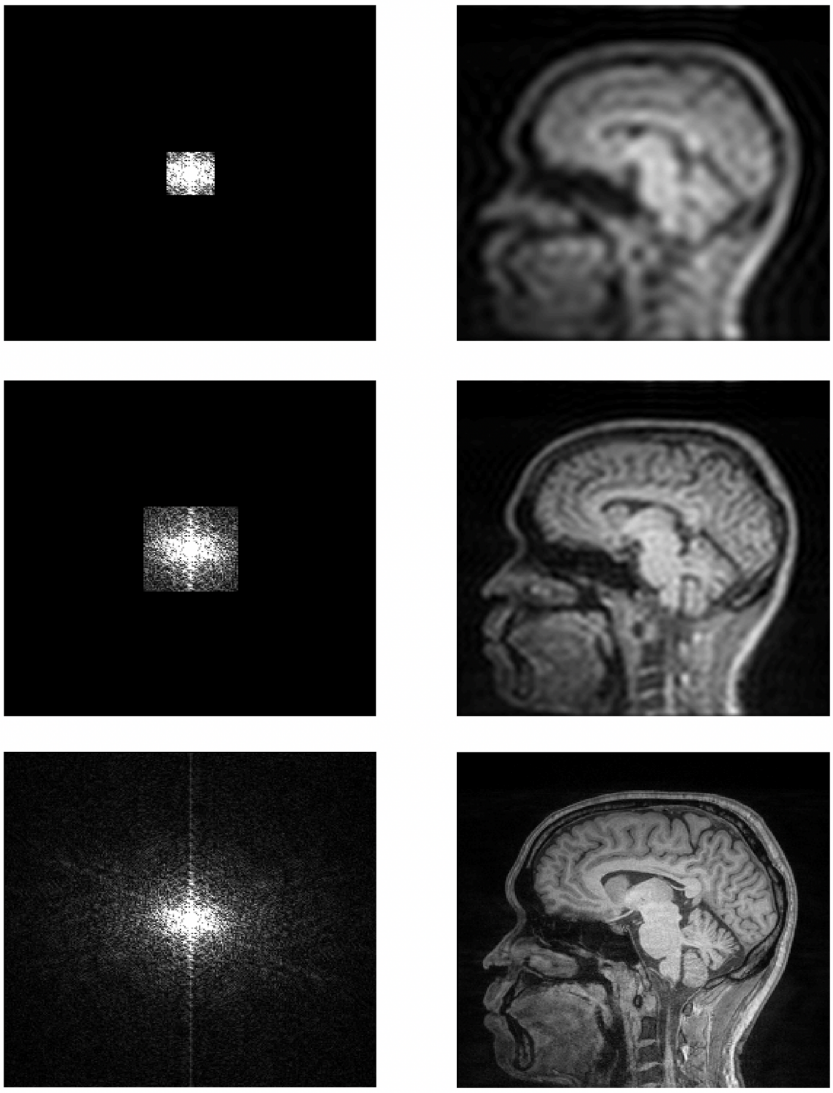

Figure 5: Relation between extent of k-space coverage and spatial resolution of the reconstructed images. In the left column, the depicted Fourier transforms differ in the extent of k-space that is covered. The areas of k-space covered in the first and second rows are 6.25% and 25%, respectively, of the area covered in the third row. The central portions of k-space contain information from low spatial frequencies, whereas the outer parts of k-space contain information from higher spatial frequencies. The images reconstructed from each of the Fourier transforms are shown in the right column. As the k-space coverage increases to include higher spatial frequencies, the reconstructed images include finer spatial details and thus exhibit higher spatial resolution.

In addition to Fourier-based image reconstruction, modern MRI systems are making increasing use of generalized reconstruction approaches that take can advantage of multiple channels of information and effectively integrate prior information about the object of interest (Feng et al., 2017; Hamilton, Franson, & Seiberlich, 2017; Lundervold & Lundervold, 2019).

Researchers can use these advanced reconstruction methods to shorten the time required for image acquisition, achieve gains in temporal or spatial resolution, or minimize artifacts.

The Flexibility of MRI

One of the factors that distinguishes MRI from other imaging methods is the ability to program the MRI system to implement a wide range of imaging modalites, where each modality offers unique information about the biological sample of interest. This ability stems from the fact that both the amplitude and phase of the magnetization can be manipulated to highlight different biological phenomenon. By directly manipulating the magnetization within the object, the MRI system is essentially modifying the object that will be imaged. Modern MRI systems provide researchers with great flexibility in manipulating the spins through specification of the timing, amplitude, and phase of both the RF and gradient fields using a pulse sequence programming environment. Additional flexibility and capabilities can be achieved with advanced hardware (such as multiple transmit and receive channels) and a wide range of image reconstruction and analysis methods.

The Use of Phase in MRI

In the above discussion of contrast, the main focus was on adjusting pulse sequence parameters (e.g. TR and TE) to manipulate the amplitude of the magnetization to reflect differences in the T_1, T_2, and proton density parameters. For a wide range of MRI applications, it is also important to understand how the phase of the magnetization can provide useful information. To provide a basic understanding, we first recall that magnetization precesses at the local Larmor frequency $f(x, y, z) = \frac{\gamma}{2\pi}(B_0 + \Delta B(x, y, z))$ where $\Delta B(x, y, z)$ represents any deviation in the magnetic field from the uniform field value of B_0. This deviation can reflect a number of factors, such as (1) additive gradient fields that are controlled by the user, (2) non-idealities in the MRI hardware, and (3) the presence of naturally occurring inhomogeneities in the magnetic field.

In some MRI applications, the difference in phase between different magnetization populations is directly detected with the MRI hardware and converted into a quantity of interest.

For example, in phase contrast angiography (PCA), the phase of the magnetization is proportional to the velocity of blood. This relationship is accomplished through the use of a time-varying gradient field. In Figure 6a, we depict a stationary spin shown in black and a moving spin show in red. At the start of the experiment, both spins are located at the same physical location and exhibit a phase angle $\phi(0) = 0$. A negative linear gradient along the x-axis is applied during the first half of the experiment (from time 0 to time T). Because both spins are at positive x locations they experience a negative field offset $\Delta B_z(x) < 0$, which causes them to precess more slowly than a spin located at the origin. This causes them both to accumulate a positive phase. In addition, the moving spin flows into a region where the magnetic field grows progressively weaker and thus precesses even more slowly than the stationary spin, such that it has a larger net phase at time T, with $\phi(T) = 135$ for the moving spin and $\phi(T) = 90$ for the stationary spin. In the second half of the experiment (from time T to 2T), we reverse the sign of the linear gradient, so that both spins now experience a positive field offset $\Delta B_z(x) > 0$, causing both to precess more quickly than a spin located at the origin. For the stationary spin, the effects of the positive field offset during the second half of the experiment exactly cancels out the effects of the negative field offset during the first half. As a result, the net phase of this spin is zero at the end of the experiment ($\phi(2T) = 0$). In contrast, the moving spin keeps moving into a region with increasingly stronger magnetic fields and so the effects of the positive field offset during the second half of the experiment overcompensate for the effects of the negative field offset during the first half. At the end of the experiment, the moving spin has acquired a net phase $\phi(2T) = -45$ that is proportional to its velocity. Figure 6b shows the an example use of PCA to assess blood flow in the internal carotid and vertebral arteries.

Another imaging approach that depends directly on the measurement of phase is susceptibility weighted imaging (SWI). Localized changes in magnetic susceptibility $\chi(x, y, z)$ give rise to changes in the local magnetic fields $\Delta B(x, y, z)$ that can be characterized by the local phase $\phi(x, y, z) = \gamma \Delta B(x, y, z)\text{TE}$ measured at the echo time TE. SWI has been primarily used to examine the presence of iron deposition in the brain and to characterize venous oxygenation, which is related to the presence of deoxyhemoglobin (see section below on Functional Imaging for additional discussion of the magnetic properties of deoxyhemoglobin). A

review of the clinical applications can be found in (S. Liu et al., 2017).

For other applications, phase differences are indirectly detected through their effects on the net transverse magnetization that is detected. In Figure 7(a), we consider the presence of static magnetic field inhomogeneities on both phase differences and the resulting MRI signal. At the start of the experiment ($t = 0$), the spins in the transverse plane are aligned and the net MRI signal is equal to the vector sum of the spins (indicated by the blue arrow). In the presence of moderate spatial inhomogeneities in the magnetic field (indicated by variations in color in the upper diagram), the spins experience slightly different fields and precess at different frequencies. As a result, at the measurement time ($t = \text{TE}$), the spins have undergone a moderate degree of dephasing such that the vector sum has decreased from its initial value. This is manifests as a decrease in the measured MRI signal. In the lower half of panel (a), the degree of field inhomogeneity is much greater and so there will be more dephasing of the spins. This leads to a more pronounced decrease in the MRI signal. In pulse sequences that make use of this effect, the amplitude of the MRI signal serves an indicator of the degree of magnetic field inhomogeneity at each location. An application of this effect to functional imaging of the brain is shown in Figure 7(b) and discussed in a later section.

The relation between dephasing of spins and the amplitude of the MRI signal can also be used to assess diffusion in biological tissues. In Figure 8(a) we consider two spins diffusing along the x-axis. At the start of the experiment, both spins are located at the same physical location and exhibit a phase angle $\phi(0) = 0$. A negative linear gradient along the x-axis is applied during the first half of the experiment (from time 0 to time T). At time T both spins have accrued a positive phase since they are precessing in the presence of a negative field offset. In the second half of the experiment, the sign of the gradient is flipped such that both spins now experience a positive field offset. However, because of the random motion of the spins, the positive field offset does not cancel out the effects of the negative field offset. As a result, both spins have accrued a net phase at time $2T$. If we imagine a collection of many spins diffusing, then there will be a distribution of phases at the end of the experiment, where the width of the distribution increases with diffusivity. A greater dispersion of phases corresponds to a higher degree of dephasing, leading to a smaller MRI signal. For a diffusion

weighted experiment, the signal amplitude is given by $S = S_0 \exp(-bD)$ where S_0 is the signal amplitude without diffusion weighting, D denotes diffusivity, and b is known as the b value, which depends on the timing and amplitude of the applied gradients. Applications of diffusion MRI are discussed in a later section and some example images are shown in Figure 8(b,c).

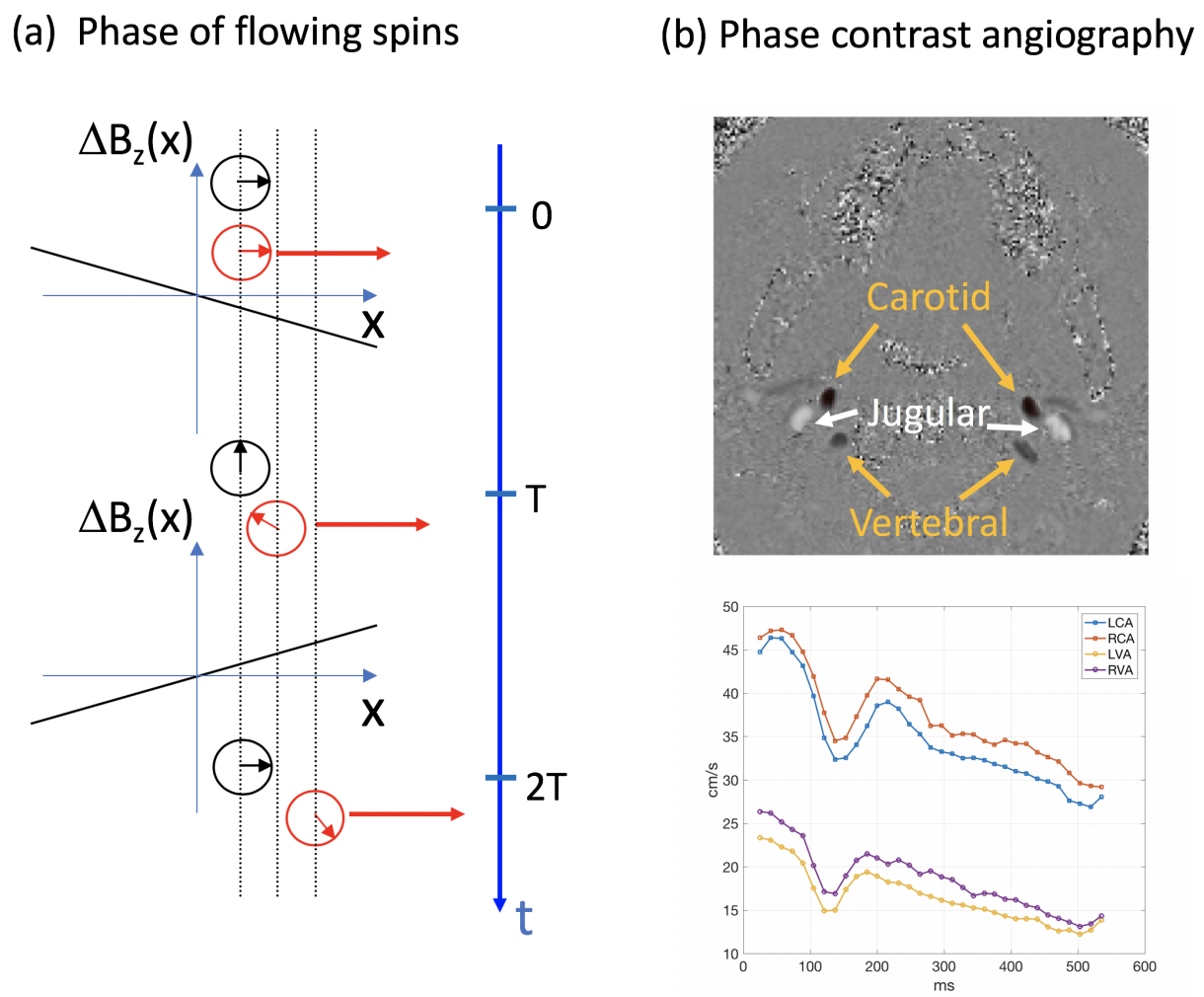

Figure 6: (a) Time-varying gradients can be used to measure the velocity of moving spins. The black spin is stationary while the red spin is moving in the $+x$ direction with a constant velocity v. In the first half of the experiment ($t \in [0, T]$), a negative gradient is applied such that both spins experience a negative field offset that causes them to precess more slowly (and accrue positive phase since the precession is clockwise) than a spin located at the origin. The moving spin flows into a region where the magnetic field grows progressively weaker and thus precesses even more slowly than the stationary spin. At time T the stationary and moving spins have phases of 90 and 135 degrees, respectively. The sign of the gradient is reversed for the second half of the experiment ($t \in [T, 2T]$). For the stationary spin, the effects of the positive field offset during the second half of the experiment exactly cancels out the effects of the negative field offset during the first half so that it has zero phase at the end of the experiment. In contrast, the moving spin keeps moving into a region with increasingly stronger magnetic fields. The effects of the positive field offset during the second half of the experiment overcompensate for the effects of the negative field offset during the first half, such that the spin has accrued a net phase of -45 degrees at the end of the experiment. This phase is directly proportional to its velocity. (b) The phase contrast angiography (PCA) image in the top plot depicts flow towards the brain through the internal carotid and vertebral arteries, indicated with the black shading. Flow away from the brain through the internal jugular veins is indicated with the white shading. The time-varying flow velocities during the initial portion of the cardiac cycle are shown in the bottom plot for the left and right carotid (LCA, RCA) and vertebral (LVA, RVA) arteries.

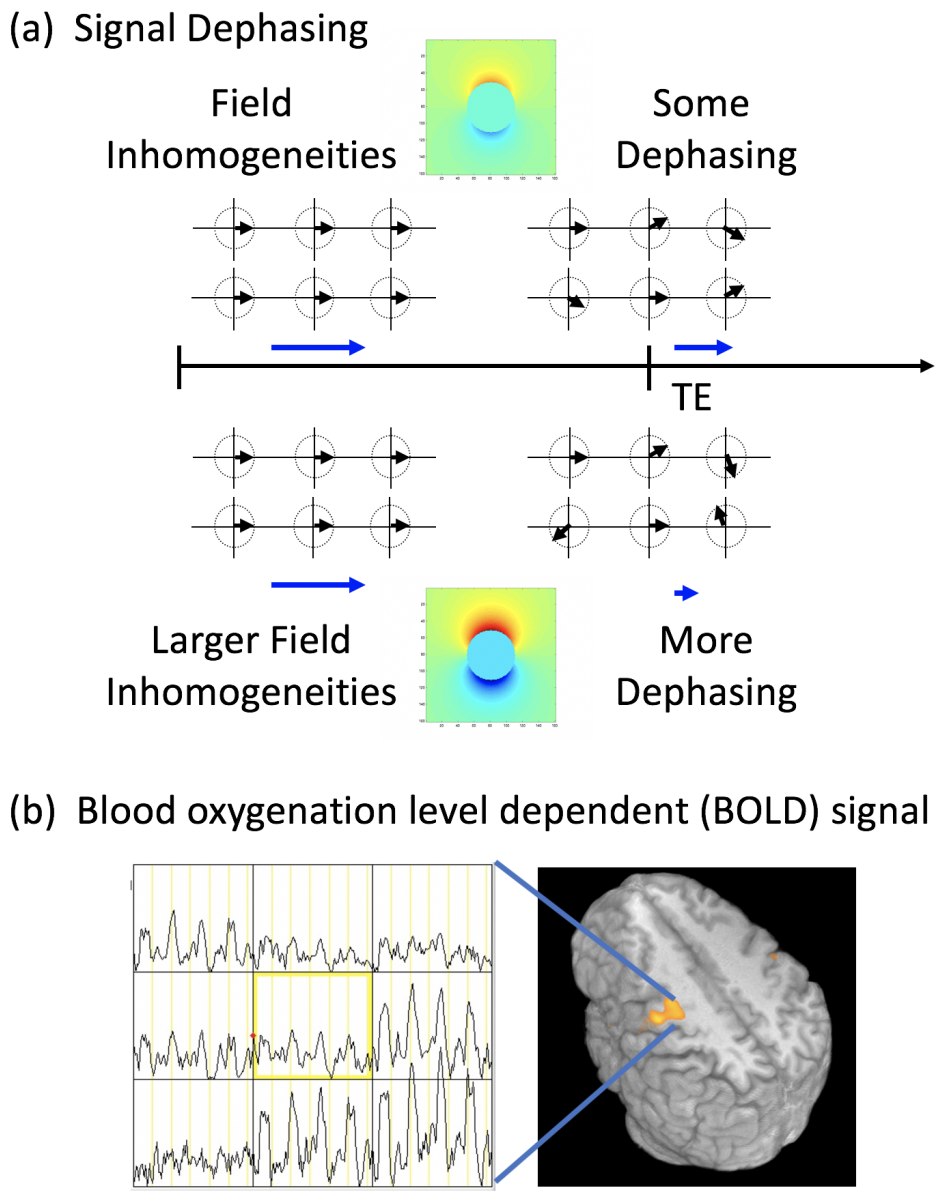

Figure 7: (a) Signal dephasing and the presence of magnetic field inhomogeneities. At time $t = 0$, the spins are in phase and the resulting MRI signal (vector sum of the spins) is indicated by the blue arrow. In the presence of moderate spatial inhomogeneities in the magnetic field (upper diagram), the spins experience slightly different fields and precess at different frequencies. Thus at the measurement time $t = \text{TE}$, there will moderate dephasing of the spins leading to a decrease in the MRI signal, as indicated by the shorter blue arrow. In the lower half of the panel, the degree of field inhomogeneity is much greater and so there will be more dephasing of the spins. This leads to a more pronounced decrease in the MRI signal. (b) In this example, the subject tapped the fingers of his right hand. This resulted in blood oxygenation level dependent (BOLD) signal changes in the left motor cortex (indicated by the yellow colors). Representative BOLD time courses from this region are shown on the left. Finger tapping leads to an increase in blood oxygenation, which leads to a decrease in signal dephasing and an increase in the MRI signal.

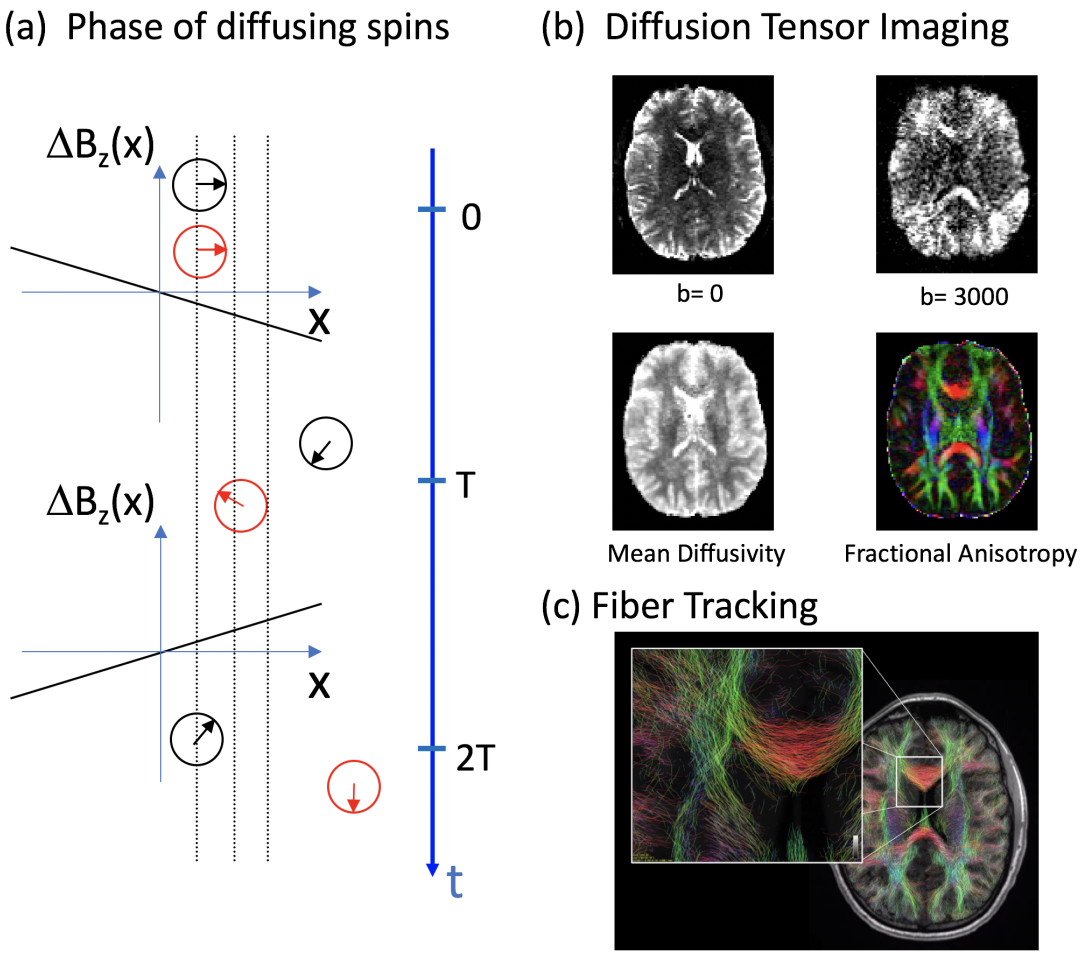

Figure 8: (a) Time-varying gradients can be used to assess diffusivity. In this example, both spins start off at the same position along the x-axis and then move randomly in the presence of the gradient field. In the first half of the experiment ($t \in [0, T]$), a negative gradient is applied such that both spins experience a negative field offset that causes them to precess more slowly (and accrue positive phase since the precession is clockwise) than a spin located at the origin. The sign of the gradient is flipped for the second half of the experiment ($t \in [T, 2T]$). Due to the random motion of the spins, the positive field offset during the second half of the experiment does not cancel out for the effects of the negative field offset during the first half. As a result, both spins have acquired a net phase. If we imagine a collection of many spins diffusing, then there will be a distribution of phases at the end of the experiment, where the width of the distribution increases with diffusivity. (b) The top row show images with no additional diffusion weighting (b = 0) and substantial diffusion weighting (b = 3000), where the direction of the diffusion gradients for the b=3000 image is largely perpendicular to the displayed image slice. As a result, the brighter parts of the image indicate regions where the primary direction of diffusion lies within the image plane. By combining measures from images acquired with different diffusion gradient directions, it is possible to obtain a map of the mean diffusivity (lower left), where the brightness of the image is proportional to diffusivity. A map of fractional anisotropy can also be obtained (lower right), where the colors red, green, and blue indicate fibers running in the left-right, anterior-posterior, and superior-inferior directions, respectively, and the brightness indicates the degree of anisotropy of the diffusion tensor at each location. (c) Estimates of the primary direction of diffusion at each location can be combined to form maps of the white matter fibers.

MRI Applications

Imaging of Anatomical Structure

One of the primary applications of MRI is the imaging of anatomical structure to quantify the size of biological objects and to detect abnormalities. As discussed above, differences in the relaxation times of various tissues can be used to create images with different contrasts. Figure 2(b) shows the same brain imaged using the spin-echo pulse sequence with different sets of pulse sequence parameters, each designed to achieved a specific type of contrast between gray matter, white matter, and cerebrospinal fluid. The proton density, T_1, and T_2 values of the different tissue types are listed in the table below the images.

In the T_1-weighted image, the pulse sequence is designed to highlight the differences between the T_1 values of gray matter and white matter, with white matter appearing slightly brighter than the gray matter since it has a shorter T_1 and thus recovers more quickly. Note that cerebrospinal fluid (CSF) appears dark in this image since it has a long T_1 and takes much longer to recover than either white or gray matter. In the density-weighted image, the brightness of the tissues is proportional to their relative proton densities, such that CSF appears the brightest and white matter is the least bright. For the T_2-weighted image, the pulse sequence is designed to highlight the differences between the T_1 values of gray matter and white matter, with white matter appearing darker than gray matter since it has a shorter T_2 and thus decays more quickly. CSF appears very bright in this image because it decays very slowly with a long T_2.

In some instances, it is advantageous to inject a contrast agent to alter the relaxation rates of the spins and achieve greater contrast. For example, injection of a gadolinium-based T_1 contrast agent that accumulates in a tumor can shorten the T_1 in the cancerous tissue, thus enhancing the signal intensity and facilitating detection of the tumor (Sinharay & Pagel, 2016; De León-Rodríguez, Martins, Pinho, Rofsky, & Sherry, 2015). Additional applications of contrast agents are discussed below in the section on imaging of physiology.

Diffusion tensor imaging (DTI) can be used to assess the anisotropy of biological structures (Mori & Tournier, 2013). In a DTI experiment, gradients are used to sensitive the measurement to the random motion of the spins. In the simple example of Figure 8(a),

gradients along the x-axis are used to measure diffusivity in the x-direction. By using a combination of gradients along all three axes (x, y, z), the diffusivity in any arbitrary direction can be measured. The upper right-hand image (b = 3000) in Figure 8(b) shows an example of an image obtained when the gradients are sensitized to diffusion in a direction that is nearly perpendicular to the image plane. For comparison, the upper left-hand image (b = 0) is obtained without additional diffusion gradients. The signal in brain regions for which the primary direction of diffusion is perpendicular to the imaging plane will be significantly attenuated (as compared to the (b=0) image), while the signal in brain regions for which the primary direction of diffusion lies within the image plane will undergo minimal attenuation. Thus, the brighter looking regions in the (b = 3000) image correspond to brain regions where the primary direction of diffusion is largely within the plane of the image.

A typical DTI experiment will acquire a collection of images using diffusion gradients along many different directions. These images can then be combined to form an estimate of mean diffusivity, which is the diffusivity averaged over all the directions. In the lower lefthand image in Figure 8(b), the brighter areas reflect the higher mean diffusivity of the cerebral spinal fluid in the sulci and ventricles. The images acquired with different diffusion gradient directions can also provide estimates of the primary direction of diffusion in anisotropic tissues such as the white matter fibers in the brain. The lower righthand image in Figure 8(b) depicts the fractional anisotropy of the tissue where the colors indicate the primary direction of diffusion and the brightness of the colors reflects the degree of anisotropy. The estimates of the primary diffusion direction can be further used to form estimates of the paths followed by the white matter fibers, as shown in Figure 8(c). This process is referred to as fiber tracking (Mori & Tournier, 2013).

Here we have focused on the use of DTI to characterize anisotropy in the brain. Other applications of DTI include characterizing the architecture of muscle fibers in the heart and the musculoskeletal system (Mekkaoui, Reese, Jackowski, Bhat, & Sosnovik, 2017; Budzik et al., 2014).

Imaging of Physiology

As discussed above, phase information in MRI can be used to quantify the velocity of flowing spins. As an application of this approach, phase contrast angiography (PCA) is widely used to characterize blood flow in the larger arteries and veins. In the upper part of Figure 6b the PCA image depicts blood flowing towards the brain through the carotid and vertebral arteries (indicated in black) and blood flowing away from the brain through the jugular veins (indicated in white). In the lower half of the figure, the velocities in the carotid and vertebral arteries at different time points in the cardiac cycle are shown. In this example, flow encoding gradients in a single direction roughly parallel to the vessels were used to characterize the velocity. In general, all three components of the velocity vector can be measured by acquiring three sets of images where each set uses flow encoding gradients in one of three orthogonal directions. Extensions of the PCA approach have been used to characterize the complex patterns of blood flow in the chambers of the heart (Edelman & Koktzoglou, 2019).

Most of the other MRI approaches for characterizing blood flow and perfusion can be understood using the basic concepts introduced above. For example, in time of flight (TOF) angiography, short repetition time (TR) acquisitions are used to differentiate flowing blood from static tissue. Because of the short TR, the longitudinal component of the static tissue magnetization does not have time to fully recover. As a result, static tissue appears relatively dark. In contrast, blood flow delivers fully relaxed magnetization into the imaging volume, and the flowing blood magnetization experiences fewer RF excitations as compared to the background tissue. Due to these factors, blood appears relatively bright in the TOF angiogram (Saloner, 1995).

Exogenous contrast agents can be used to enable the characterization of blood flow and perfusion. In contrast-enhanced angiography, the shorter T_1 of an intravenously injected gadolinium-based agent increases the intensity of the MR signal in blood and thus facilitates visualization of the vasculature (Riederer, Stinson, & Weavers, 2018). In Dynamic Contrast-Enhanced (DCE) imaging, dynamic changes in T_1 measured after the bolus injection of a contrast agent are used to form estimates of physiological parameters that are related to blood flow and vascular permeability. In a related method known as Dynamic Susceptibility

Contrast (DSC), the T_2 and T_2^* shortening properties of gadolinium are used to characterize cerebral blood volume (CBV) and cerebral blood flow (CBF) (Jahng, Li, Ostergaard, & Calamante, 2014).

In arterial spin labeling (ASL) MRI, RF pulses are used to invert the longitudinal magnetization of flowing blood while it is still in the feeding arteries (see Figure 9(a)) (Alsop et al., 2015; T. T. Liu & Brown, 2007). While there are various methods that can be used, one straightforward approach is to apply a spatially selective inversion pulse that inverts blood in a region that covers the feeding arteries, as depicted by the solid green box in Figure 9(a). These inverted spins serve as an intrinsic source of contrast which flows into the imaging region. An image acquired before the spins have fully relaxed will reflect the delivery of blood to the tissue (referred to as the tag image). In practice, a second image (known as the control image) in which the magnetization of flowing blood is fully relaxed as it flows into the imaging region is also acquired. The subtraction of the control and tag images cancels out the static tissue contributions and reflects the blood magnetization that has been delivered. With proper calibration, this difference image can be converted into a map of cerebral blood flow in physiological units, as shown in Figure 9(b). Extensions of this approach include: (1) performing dynamic subtraction of the control and tag images to characterize the functional CBF response to brain activity, as shown in Figure 9(c) and (2) the use of clever encoding methods to characterize the vascular territories supplied by each artery (van Osch et al., 2018; Kansagra & Wong, 2008)

Variants of ASL can also be used to assess the oxygenation of blood in the venous system. In these methods, the blood signal in the venous system is first distinguished from the MR signals from blood in the arterial compartments and the surrounding tissue. The T_2 relaxation rate of the venous blood is then characterized and used to estimate venous oxygenation based on the relation between T_2 and oxygenation. When combined with measures of CBF, the oxygenation measures can be used to estimate the rate of oxygen metabolism (Hernandez-Garcia, Lahiri, & Schollenberger, 2019).

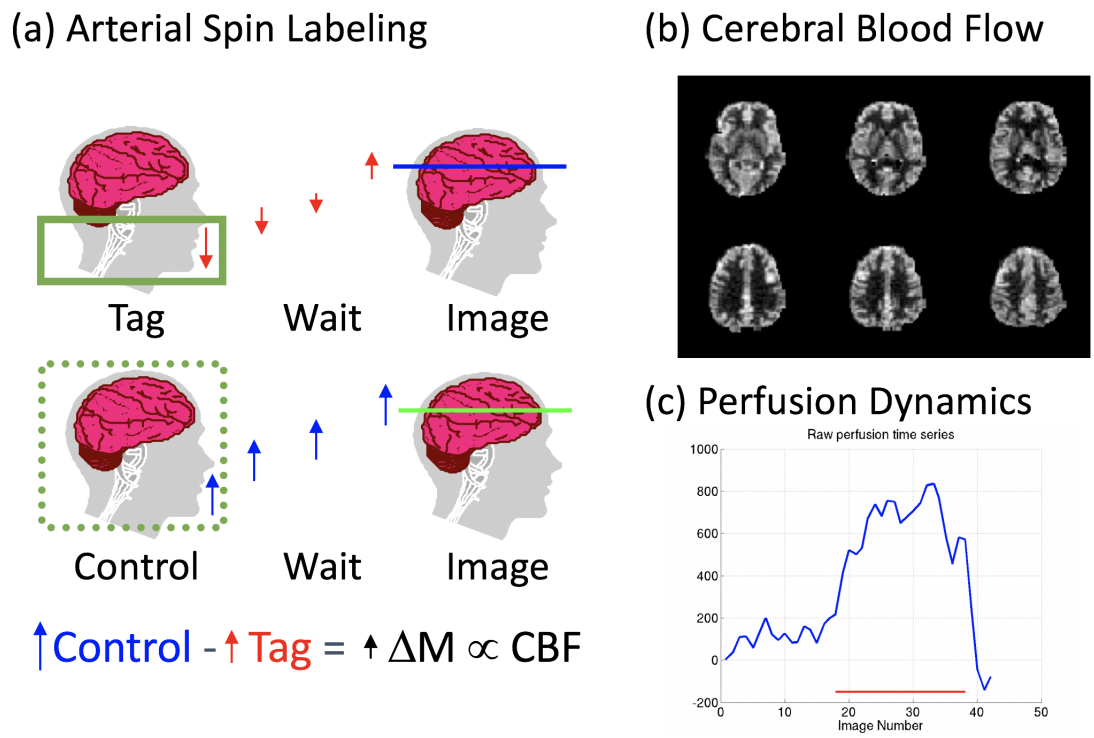

Figure 9: (a) An arterial spin labeling (ASL) MRI experiment typically consists of tag and control sections. In each tag section, spins in the feeding arteries undergo magnetic inversion and then flow into the imaging region while undergoing longitudinal relaxation. After waiting for the spins to arrive in the imaging region, an image is acquired before the spins have fully relaxed. In each control section, fully relaxed spins flow into the imaging region and an image is acquired. The difference of the control and tag images is proportional to cerebral blood flow. (b) Cerebral blood flow maps are generated by taking the average difference of the control and tag images. (c) In most ASL experiments, multiple control and tag images are acquired in an interleaved fashion. Temporal changes in perfusion can be estimated by taking the running difference of the control and tag images. The blue curve shows the perfusion response (arbitrary units) to a visual stimulus, where the time period during which the stimulus was applied is indicated by the red bar.

Imaging of Function

As noted in the previous section, ASL MRI can be used to measure functional changes in blood flow related to brain activity. However, the predominant MRI method for the characterization of brain function is based on what is known as the blood oxygenation level dependent (BOLD) signal (Matthews & Jezzard, 2004). Functional brain imaging based on the BOLD signal is commonly referred to as BOLD functional MRI (fMRI). The BOLD signal can be understood by revisiting the concept presented in Figure 7(a), which described the dependence of the amplitude of the MRI signal on the dephasing of the spins. In Figure 7(a),

the dephasing of the spins was simply stated to be a consequence of the presence of spatial inhomogeneities in the magnetic field. In BOLD fMRI, the inhomogeneities are due to the presence of iron atoms that lie at the center of the hemoglobin molecule. When oxygen binds to the hemoglobin molecule in the lungs to form oxyhemoglobin, the oxygen atoms act to shield the surrounding environment from the magnetic effects of the iron atom. When the oxygen is used for metabolism (leading to an increase in deoxyhemoglobin), the shielding is reduced and the iron atom can perturb the magnetic field of the surrounding environment. Since a greater degree of perturbation leads to an increase in the inhomogeneity of the fields, it would seem that an increase in brain activity would lead to a greater use of oxygen, a reduction in shielding, more dephasing, and hence a decrease in the MRI signal. The surprising finding is that in most cases, one observes an increase in the MRI signal with brain activity. It turns out that when the brain increases blood flow to support brain activity it overcompensates such that the percent increase in blood flow is two to three times the percent increase in metabolism. As a result, the brain delivers more oxygen than is needed, so that the deoyxhemoglobin content actually decreases, leading to a decrease in signal dephasing and an increase in the MRI signal. An example of the BOLD fMRI response to a finger tapping task is shown in Figure 7(b). Since the first observation of the BOLD signal in humans in 1992, the use of BOLD fMRI has revolutionized the study of the human brain due to the non-invasiveness of the method (Rosen & Savoy, 2012).

Term	**Description**
ASL	Arterial Spin Labeling
BOLD	Blood Oxygenation Level Dependent
$\mathbf{B}_0$	Main magnetic field vector
B_0	Main magnetic field strength
$\mathbf{B}_1$	RF magnetic field vector
CBV	Cerebral Blood Volume
CBF	Cerebral Blood Flow
DCE	Dynamic Contrast-Enhanced
DSC	Dynamic Susceptibility Contrast
DTI	Diffusion Tensor Imaging
fMRI	Functional MRI
γ	Gyromagnetic ratio
$\mathbf{M}$	Magnetization vector
M_0	Equlibrium magnetization
M_z	Longitudinal component of magnetization
M_{xy}	Transverse component of magnetization
PCA	Phase Contrast Angiography
RF	Radiofrequency
SWI	Susceptibility Weighted Imaging
TE	Echo Time
TI	Inversion Time
TOF	Time of Flight
TR	Repetition Time
T_1	Longitudinal relaxation time constant
T_2	Transverse relaxation time constant
T_2^*	Effective transverse relaxation time constant

Table 1: Glossary of Terms

ACKNOWLEDGEMENTS

This work was supported in part by NIH grant R21MH112155. I would like to thank Yashar Behzadi, Robert Bussell, Richard Buxton, Aaron Jacobson, Wen-Ming Luh, Khaled Restom, David Shin, and Eric Wong for kindly providing images and data that were used to construct the figures. I have no conflicts of interest to declare with respect to the content of this article.

CONCLUSIONS

MRI is a powerful and widely used tool for both clinical and research applications. This paper has focused on providing the reader with a brief introduction to the fundamental concepts employed in MRI and demonstrating how these concepts are utilized in a few widely used methods. While the examples in this paper have been limited to MRI of the human brain, the same principles and concepts can be applied and extended to MRI of other organs and animals. It is hoped that the motivated reader will find this paper to be a useful stepping stone to the vast and remarkable world of MRI.

References

Alsop, D. C., Detre, J. A., Golay, X., Günther, M., Hendrikse, J., Hernandez-Garcia, L., ... Zaharchuk, G. (2015, January). Recommended implementation of arterial spin-labeled perfusion MRI for clinical applications: A consensus of the ISMRM perfusion study group and the European consortium for ASL in dementia. *Magnetic resonance in medicine : official journal of the Society of Magnetic Resonance in Medicine / Society of Magnetic Resonance in Medicine*, *73*(1), 102–116.

Budzik, J.-F., Balbi, V., Verclytte, S., Pansini, V., Le Thuc, V., & Cotten, A. (2014, May). Diffusion tensor imaging in musculoskeletal disorders. *Radiographics : a review publication of the Radiological Society of North America, Inc*, *34*(3), E56–72.

De León-Rodríguez, L. M., Martins, A. F., Pinho, M. C., Rofsky, N. M., & Sherry, A. D. (2015, September). Basic MR relaxation mechanisms and contrast agent design. *Journal of magnetic resonance imaging : JMRI*, *42*(3), 545–565.

Edelman, R. R., & Koktzoglou, I. (2019, February). Noncontrast MR angiography: An update. *Journal of magnetic resonance imaging : JMRI*, *49*(2), 355–373.

Feng, L., Benkert, T., Block, K. T., Sodickson, D. K., Otazo, R., & Chandarana, H. (2017, April). Compressed sensing for body MRI. *Journal of magnetic resonance imaging : JMRI*, *45*(4), 966–987.

Hamilton, J., Franson, D., & Seiberlich, N. (2017, August). Recent advances in parallel imaging for MRI. *Progress in nuclear magnetic resonance spectroscopy*, *101*, 71–95.

Hargreaves, B. A. (2012, December). Rapid gradient-echo imaging. *Journal of magnetic resonance imaging : JMRI*, *36*(6), 1300–1313.

Hernandez-Garcia, L., Lahiri, A., & Schollenberger, J. (2019, February). Recent progress in ASL. *NeuroImage*, *187*, 3–16.

Jahng, G.-H., Li, K.-L., Ostergaard, L., & Calamante, F. (2014, October). Perfusion Magnetic Resonance Imaging: A Comprehensive Update on Principles and Techniques. *Korean Journal of Radiology*, *15*(5), 554–577.

Kansagra, A. P., & Wong, E. C. (2008, September). Mapping of vertebral artery perfusion territories using arterial spin labeling MRI. *Journal of magnetic resonance imaging : JMRI*, *28*(3), 762–766.

Liu, S., Buch, S., Chen, Y., Choi, H.-S., Dai, Y., Habib, C., ... Haacke, E. M. (2017, April). Susceptibility-weighted imaging: current status and future directions. *NMR in Biomedicine*, *30*(4), e3552.

Liu, T. T., & Brown, G. G. (2007, May). Measurement of cerebral perfusion with arterial spin labeling: Part 1. Methods. *Journal of the International Neuropsychological Society : JINS*, *13*(3), 517–525.

Lundervold, A. S., & Lundervold, A. (2019, May). An overview of deep learning in medical imaging focusing on MRI. *Zeitschrift fur medizinische Physik*, *29*(2), 102–127.

Matthews, P. M., & Jezzard, P. (2004, January). Functional magnetic resonance imaging. *Journal of neurology, neurosurgery, and psychiatry*, *75*(1), 6–12.

Mekkaoui, C., Reese, T. G., Jackowski, M. P., Bhat, H., & Sosnovik, D. E. (2017, March). Diffusion MRI in the heart. *NMR in Biomedicine*, *30*(3), e3426.

Mori, S., & Tournier, J. D. (2013). *Introduction to Diffusion Tensor Imaging: And Higher*

Order Models. Oxford, UK: Elsevier Science.

Plewes, D. B. (1994, November). The AAPM/RSNA physics tutorial for residents. Contrast mechanisms in spin-echo MR imaging. *Radiographics : a review publication of the Radiological Society of North America, Inc*, *14*(6), 1389–404– quiz 1405–6.

Riederer, S. J., Stinson, E. G., & Weavers, P. T. (2018, January). Technical Aspects of Contrast-enhanced MR Angiography: Current Status and New Applications. *Magnetic resonance in medical sciences : MRMS : an official journal of Japan Society of Magnetic Resonance in Medicine*, *17*(1), 3–12.

Rosen, B. R., & Savoy, R. L. (2012, August). fMRI at 20: has it changed the world? *NeuroImage*, *62*(2), 1316–1324.

Saloner, D. (1995, March). The AAPM/RSNA physics tutorial for residents. An introduction to MR angiography. *Radiographics : a review publication of the Radiological Society of North America, Inc*, *15*(2), 453–465.

Saranathan, M., Worters, P. W., Rettmann, D. W., Winegar, B., & Becker, J. (2017, December). Physics for clinicians: Fluid-attenuated inversion recovery (FLAIR) and double inversion recovery (DIR) Imaging. *Journal of magnetic resonance imaging : JMRI*, *46*(6), 1590–1600.

Sinharay, S., & Pagel, M. D. (2016, June). Advances in Magnetic Resonance Imaging Contrast Agents for Biomarker Detection. *Annual review of analytical chemistry (Palo Alto, Calif.)*, *9*(1), 95–115.

van Osch, M. J., Teeuwisse, W. M., Chen, Z., Suzuki, Y., Helle, M., & Schmid, S. (2018, September). Advances in arterial spin labelling MRI methods for measuring perfusion and collateral flow. *Journal of cerebral blood flow and metabolism : official journal of the International Society of Cerebral Blood Flow and Metabolism*, *38*(9), 1461–1480.

FURTHER READING

The website `http://mriquestions.com/index.html` is an excellent on-line resource for those wishing to learn more about MRI. A collection of educational videos hosted by the International Society for Magnetic Resonance in Medicine can be found at

https://www.ismrm.org/online-education-program/